https://doi.org/10.1016/j.ica.2017.08.030

Strain Alleviation in an Isomorphous Series of Lanthanide 2-nitroterephthalates $[Ln_2(TPNO_2)_3(H_2O)_2]\cdot 2H_2O$ (Ln = Pr – Lu, except Pm)

Ralph A. Zehnder,[*!] *Nick Fontaine,*[$] *Badwi A. Mouawad,*[§] *Jacob K. Leonard,*[§] *Matthias Zeller,*[†] *Frank R. Fronczek,*[‡] *Daniel T. de Lill,*[#] *April Ballard,*[#] *Daniel Bonnette,*[§] *Aaron Head,*[$] *Krishna Ghimire,*[$] *Jordan N. Welch,*[§] *Elee R. Barber,*[$] *Jared M. Murray,*[^] *Christian Dempsey,*[⊥] *James Jenkins,*[!] *Gregory Jackson,*[>] *Mary Tokunboh,*[$] *Stevie R. Bach,*[§] *and Jaimie A. Treadway Harris,*[§]

[!]Department of Chemistry & Biochemistry, [⊥]Department of Physics, [>]Department of Biology, Angelo State University, San Angelo, TX 76909, [§]Department of Biology, [^]Department of Psychology [$]College of Pharmacy, University of Louisiana at Monroe, Monroe, LA 71209, [†] Department of Chemistry, Purdue University, West Lafayette, IN 47907, [‡]Department of Chemistry, Louisiana State University, Baton Rouge, LA 70803, and [#]Department of Chemistry & Biochemistry, Florida Atlantic University, Boca Raton, FL 33431

*Author to whom correspondence should be addressed. Angelo State University, Department of Chemistry & Biochemistry, ASU Station #10892, San Angelo, TX 76909. Phone: (+1) 325-486-6662. E-mail: ralph.zehnder@angelo.edu. Fax (+1) 325-942-2184.

Abstract

An extended series of trivalent lanthanide 2-nitroterephthalates, $[Ln_2(TPNO_2)_3(H_2O)_2]\cdot 2H_2O$, (Ln = Pr through Lu, except Pm) were synthesized hydrothermally from Ln_2O_3 and 2-nitroterephthalic acid (H_2TPNO_2) at 170˚C in Teflon lined Parr steel autoclaves, and were characterized via single crystal X-ray diffraction, powder X-ray diffraction, FT-IR spectroscopy, elemental analyses, and thermogravimetric analyses.

All $[Ln_2(TPNO_2)_3(H_2O)_2]\cdot 2H_2O$ coordination polymers are isomorphous, crystallizing in the monoclinic crystal system with space group *C*2/c. The metal centers in all networks possess the coordination number 8, while forming a three-dimensional extended lattice. Two metal centers form Ln_2O_{14} entities, comprising crystallographically identical LnO_8 polyhedra, connected via edge-sharing, utilizing two carboxylate O-atoms. These Ln_2O_{14} units are separated along the *a*- and *b*-axes by individual 2-nitroterephthalate linkers, while being closely connected along the *c*-axis via two carboxylate groups on each side.

Compared to small inorganic anions, the rather flexible 2-nitroterephthalate seems to allow for the unobstructed decrease in size of the LnO_8 polyhedra as Ln^{3+} ionic radii decrease towards the heavier Ln elements. Hence, the structural parameters of the crystal lattice adjust gradually without noticeable strain buildup along the series resulting in isomorphous arrangements for all

networks. The thermogravimetric and FT-IR measurements seem to confirm the structural features.

Keywords: *f*-elements; metal organic frameworks; lanthanide contraction; hydrothermal synthesis; thermogravimetric analysis

1. Introduction

Extended series of lanthanide coordination polymers sometimes exhibit disruptions in the crystal lattice as a consequence of lanthanide contraction, usually resulting in reduction of coordination numbers [1]. One important parameter that influences a three-dimensional (3D) lattice's ability to alleviate strain build up, potentially causing structural rearrangements, is the linker that determines the coordination environment of the individual lanthanide (Ln) metal center. While small rigid inorganic entities promote a structural rearrangement of the crystal lattice towards smaller ionic radii [1a-d, 2], larger more flexible spacers, usually organic in nature, assist with assembling isomorphous extended series of the corresponding lanthanide networks [3]. The elucidation of structural as well as physicochemical parameters in lanthanide frameworks allows for the prediction of important features in similar actinide analogues. It has long been demonstrated that 4*f*-coordination polymers can serve as surrogates for their corresponding 5*f*-analogues with respect to structural and physicochemical data [4].

Throughout the last decade an increasing number of *f*-elements, predominantly lanthanides, have served as coordination centers in metal organic frameworks (MOFs), enriching this new and important research area with two interesting aspects:

Firstly lanthanides exhibit interesting luminescence properties, which can be tuned by choice of ligands, rendering them as excellent candidates for light emitting systems such as LEDs,

LASERs, etc. [3a, 5]. Secondly, lanthanide coordination polymers generally possess larger coordination numbers than observed for *d*-element MOFs, often resulting in unique network topologies [6]. Expanding MOF research by incorporating 4*f* and 5*f* elements may assist with future designs of potential nuclear waste matrices [5g, 7].

Previously we reported the structural trends in series of lanthanide bis-hydroxychlorides, $Ln(OH)_2Cl$,[8] and lanthanide hydroxysulfates, $Ln(OH)SO_4$ [9], comparing them with less rigid systems such as hydrated lanthanide sulfates ($[Ln_2(SO_4)_3]\cdot 8H_2O$) [1d], and terephthalates, $[Ln_2(TP)_3]\cdot XH_2O$ (X = 2, 4, 6, 10) [3b, 3d-g]. While the lanthanide bis-hydroxychlorides maintain a coordination number of 8 throughout the entire series some of the unit cell parameters fluctuate immensely, which we attributed partially to the compensation of strain buildup due to reduced ionic radii for the heavier Ln-analogoues. Throughout the series of lanthanide hydroxysulfates we observed a structural rearrangement between Gd and Tb accompanied by a reduction of the coordination number from 9 to 8. In the hydrated lanthanide sulfates and terephthalates no such fluctuations of structural parameters or rearrangements were observed.

In this work we report the structural properties in a series of hydrated lanthanide 2-nitroterephthalates, $[Ln_2(TPNO_2)_3(H_2O)_2]\cdot 2H_2O$ (Ln = Pr - Lu except Pm). This series serves as an example to demonstrate how a larger degree of flexibility in spacers seems to help alleviate potential strain buildup along the series.

Various *d*-block transition metal coordination polymers incorporating 2-nitroterephthalate have been reported,[10] of which some possess properties that render them as promising candidates with regard to gas adsorption[11] as well as the accommodation of solvent molecules.[12] Other researchers described lanthanide open frameworks that incorporate the related 5-nitroisophthalate entity,[13] some of them investigating isomorphous extended series.[14] Li *et*

al. reported an extended series of binuclear lanthanide compounds, combining the 2-nitroterephthalate spacer with 4,4'-dimethyl-2,2'-bipyridine and perchlorate ions.[15] Furthermore, Severance *et al.* described the structural properties of a 3D actinide MOF in which 2-nitroterephthalate coordinates to uranyl[16] as well as a number of main group 2-nitroterephthalates.[17]

Using similar hydrothermal synthesis methods as for our previous investigations the experiments produced highly crystalline, isomorphous materials with fairly large X-ray quality single crystals. All of these coordination polymers were synthesized via hydrothermal reaction of the corresponding lanthanide(III) oxides, Ln_2O_3, with 2-nitroterephthalic acid, and they crystallize in the monoclinic crystal system. We characterized all products via single crystal- and powder X-ray diffraction analyses, thermogravimetric analyses, elemental analyses, as well as FT-IR spectroscopy.

2. Experimental

2.1. Synthesis and Characterization

2.1.1. Materials and methods

Chemicals used as starting materials were purchased from Acros Organics (H_2TPNO_2, Ce_2O_3, Sm_2O_3, Eu_2O_3, Gd_2O_3, Dy_2O_3, Ho_2O_3), Aldrich Co. (Pr_2O_3), Alfa Aesar (Nd_2O_3, Lu_2O_3), Spectrum Chemicals, as well as Strem Chemicals (Tb_2O_3, Er_2O_3, Tm_2O_3, Yb_2O_3) and were used without further purification.

2.1.2. Synthesis of $[Ln_2(TPNO_2)_3(H_2O)_2]\cdot 2H_2O$

Samples of Ln_2O_3 were weighed out and placed in Teflon liners inside Parr Acid Digestion vessels (Ln = Pr - Lu, except Pm). The larger sized Parr steel autoclaves with a volume of 45 mL were used for all experiments (model 4744). Between 0.23 and 0.28 g of lanthanide oxide (respectively 0.70 mmol) was weighed out for each reaction. Then 0.44 g (2.1 mmol) of 2-nitroterephthalic acid was added and about 15 mL of deionized water (DI-H_2O) was included. The vessels were sealed and placed in a conventional laboratory oven at 170˚C for 7 days. At the end of the heating period the vessels were taken out of the oven and allowed to cool down to ambient temperature on the lab bench. Once at room temperature the Parr vessels were opened. Solid materials, which were submerged in water, were obtained. The resulting materials were transferred into 20 mL scintillation vials. The vials were then filled with DI-H_2O, closed and shaken in order to wash the products and remove any soluble starting materials and byproducts. The products were allowed to settle down at the bottom of the vial and the water was decanted and discarded. This rinsing process was repeated three more times. The remaining products were composed of crystalline materials that all contained single crystals of X-ray quality. Small amounts of products were stored in scintillation vials with small quantities of DI-H_2O until a single crystal was chosen for X-ray structural analysis. Small samples of the remaining materials were dried at ambient temperature on the bench top. The dry samples were homogenized using a mortar and pestle and then characterized via FT-IR spectroscopy, powder XRD, and thermogravimetric analysis.

The yields ranged between 20% (Lu) and 69% (Yb) with an average of 53%.

Anal. calcd. for $[Ln_2(TPNO_2)_3(H_2O)_2]\bullet 2H_2O$: (Pr) C, 29.38%; H, 1.75%; N, 4.28%. Found C, 28.85%; H, 1.52%; N, 4.08%. (Nd) C, 29.18%; H, 1.73%; N, 4.25%. Found C, 29.70%; H,

1.80%; N, 4.23%. (Sm) C, 28.82%; H, 1.71%; N, 4.20%. Found C, 29.08%; H, 1.76%; N, 4.20%. (Eu) C, 28.73%; H, 1.71%; N, 4.19%. Found C, 28.36%; H, 1.76%; N, 4.03%. (Gd) C, 28.43%; H, 1.69%; N, 4.14%. Found C, 28.58%; H, 1.62%; N, 3.98%. (Tb) C, 28.34%; H, 1.68%; N, 4.13%. Found C, 26.69%; H, 1.53%; N, 3.64%. (Er) C, 27.88%; H, 1.66%; N, 4.06%. Found C, 26.27%; H, 1.37%; N, 3.62%. (Ho) C, 28.00%; H, 1.66%; N, 4.08%. Found C, 27.60%; H, 1.48%; N, 3.88%. (Dy) C, 28.14%; H, 1.67%; N, 4.10%. Found C, 28.23%; H, 1.49%; N, 3.96%. (Yb) C, 27.51%; H, 1.64%; N, 4.02%. Found C, 27.96%; H, 1.67%; N, 3.97%. (Tm) C, 27.79%; H, 1.65%; N, 4.05%. Found C, 27.40%; H, 1.43%; N, 3.84%. (Lu) C, 27.47%; H, 1.63%; N, 4.00%. Found C, 27.51%; H, 1.68%; N, 4.02%.

The measured values for the Tb- and Er-species are somewhat off, which can be attributed to the fact that the powder X-ray diffraction data indicated a 7% impurity of TbO_2 and a 4.9% impurity of Er_2O_3. Accounting for these impurities improves the gap between calculated and found values: (Tb ~93%) C, 26.36%; H, 1.56%; N, 3.84%. Found C, 26.69%; H, 1.53%; N, 3.64%. (Er ~95%) C, 26.49%; H, 1.58%; N, 3.86%. Found C, 26.27%; H, 1.37%; N, 3.62%.

2.1.3. Single Crystal X-ray Structure Determination

Crystals of the $[Ln_2(TPNO_2)_3(H_2O)_2]\cdot 2H_2O$, with Ln = Sm, Eu, Dy, Ho, Er and Lu, were mounted on a Mitegen 20 micron micromesh mount using a small amount of mineral oil. The data were collected on a Bruker Smart APEX charge-coupled-device (CCD) diffractometer with an Apex2 software upgrade, and an Oxford Cryostream liquid nitrogen vapor-cooling device. Data were collected at 100 K. The instrument is equipped with a graphite monochromatized MoK_α X-ray source (λ= 0.71073 Å) with MonoCap X-ray source optics. Hemispheres or spheres of data were collected using ω scans. Data collection and initial indexing and cell refinement

were handled using the APEX II software [18]. Frame integration and final cell parameter calculations were carried out using the SAINT+ software as implemented in Apex II. The data were corrected for absorption using SADABS. Intensity data for crystals of $[Ln_2(TPNO_2)_3(H_2O)_2]\cdot 2H_2O$, with Ln = Pr, Nd, Gd, Tb, Tm, and Yb were collected at 95K on a Nonius KappaCCD diffractometer equipped with an Oxford Cryosystems Cryostream sample cooler and a graphite monochromated MoK_α X-ray source (λ= 0.71073 Å). Data were collected using ϕ and ω scans and corrected for absorption using the multi-scan method using DENZO and SCALEPACK.[19]

The structures were solved either by direct methods, Patterson methods, SIR[20], or isomorphous replacement, but all structures were eventually refined in a common structural model. The monoclinic beta angle is near 90 degrees and decreases steadily by about one degree across the isomorphous series from Pr to Lu, becoming acute at Ho. Thus the nonstandard acute beta setting was used for Ho through Lu (Table 1). Structures were refined by full matrix least squares against F^2 with all reflections using Shelxl2014 and the graphical interface ShelXle.[21] Non-hydrogen atoms were refined anisotropically. One of the two 2-nitroterephthalate spacers is located on a crystallographic twofold axis, inducing 1:1 disorder of the nitro group with an H atom. The other 2-nitroterephthalate entity shows disorder of the nitro group by slight rotation around the C-N bond. The $C\text{-}NO_2$ units were restrained to be approximately planar and to have similar C-N as well as N-O bond lengths. U^{ij} components of ADPs of disordered N and O atoms were restrained to be similar, and ADPs of equivalent atoms constrained to be identical. For the Tb derivative, O5 and O5B were restrained to be approximately isotropic. H atoms attached to carbon atoms were positioned geometrically and constrained to ride on their parent atoms, with carbon hydrogen bond distances of 0.95 Å. Water H atoms were located in difference density

maps and were refined with O-H distance restraints of 0.84(2) Å. U_{iso}(H) values were set to a multiple of U_{eq}(C/O) with 1.5 for OH and 1.2 for C-H units, respectively. Complete crystallographic data, in CIF format, have been deposited with the Cambridge Crystallographic Data Centre. CCDC 1549877-1549888 contain the supplementary crystallographic data for this paper. These data can be obtained free of charge from The Cambridge Crystallographic Data Centre via www.ccdc.cam.ac.uk/data_request/cif.

Figures displaying structural motifs were created using CrystalMaker® 9.2 for Mac

2.1.4. Powder X-ray Structure Determination

Powder diffraction (XRD) data were collected on a Panalytical Empyrean X-ray diffractometer equipped with Bragg-Brentano HD optics, a sealed tube copper X-ray source (λ = 1.54178 Å), soller slits on both the incident and receiving optics sides, and a PixCel3D Medipix detector. Samples were hand-ground using an agate mortar and pestle and packed in either metal sample cups with a sample area 16 mm wide and 2 mm deep, or using silicon single crystal zero background sample holders, 16 mm wide and 0.25 mm deep (depending on sample amount available). Anti-scatter slits and divergence slits as well as masks were chosen based on sample area and starting θ angle. Data were collected between 10 and 90° in 2θ using the Panalytical Data Collector software. Purity of the multicrystalline samples was checked by Rietveld refinements against the models of the single crystal structure data sets, using the HighScore software of Panalytical. Refinement of preferred orientation was included using a spherical harmonics model. For the Er and Tb derivatives, small quantities of the respective oxides were found and included in the Rietveld fit in form of Er_2O_3 (ICSD-39185) and TbO_2 (ICSD-28846). The oxide contents refined to 4.9% for Er_2O_3, and to 6.95% for TbO_2 (by weight). No other

crystalline impurities were detected and all other $[Ln_2(TPNO_2)_3(H_2O)_2]\cdot 2H_2O$ samples were found to be phase pure by XRD. Plots of Rietveld fits for all networks are given in the SI.

2.1.5. Thermogravimetric analysis.

Thermogravimetric analyses (TGA) were performed with a TGA/DSC 1 Star system (Mettler Toledo).

A clean porcelain crucible was placed onto the balance mounted inside the TGA instrument. Under a stream of nitrogen, a blank curve was processed from 25˚C to 900˚C at 10˚C min^{-1}, and then the instrument was allowed to cool to 25˚C. Between 1.5 - 2 mg of sample were placed into the porcelain crucible and placed onto the balance mounted in the instrument. The sample was heated from room temperature to 900˚C at a rate of 10˚C min^{-1} under an N_2 atmosphere. The steps in the curves were then analyzed using either horizontal or tangential steps that determine the mass percent lost from the sample. The tangential steps were used for the elongated, less steep steps and the horizontal steps were used for the sharp, steeper steps.

TGA Plots of each coordination polymer are available in the SI and were created using the STARe Software, version 9.30 copyright by Mettler-Toledo AG 1993-2009.

2.1.6. FT-IR Spectroscopy

IR spectra were collected on a PerkinElmer Spectrum 100 FT-IR Spectrometer using KBr pellets. Spectral resolution was typically 4 cm^{-1}, and average data sets included 64 scans.

Figure 8 displaying IR spectra was created using Igor Pro 6 for Mac.

2.1.7. Elemental Analysis

Elemental analyses (EA) were performed by Midwest Microlab using an Exeter Analytical CE-440 CHNOS elemental analyzer.

Table 1. Crystal Data and Summary of Data Collection and Refinement for $[Ln_2(TPNO_2)_3(H_2O)_2]\cdot 2H_2O$, Ln = Pr-Lu (except Pm)

$[Ln_2(TPNO_2)_3(H_2O)_2]\cdot 2H_2O$	Pr	Nd	Sm	Eu	Gd	Tb	Dy	Ho
fw	981.22	987.89	1000.10	1003.32	1013.90	1017.24	1024.41	1029.26
a(Å)	16.938(2)	16.874(2)	16.814 (2)	16.783 (2)	16.794(2)	16.748(3)	16.708 (2)	16.6904 (14)
b(Å)	11.4793(10)	11.4696(14)	11.4008(15)	11.3945 (16)	11.3774(15)	11.349(2)	11.3217 (14)	11.3061 (10)
c(Å)	15.454(2)	15.4211(15)	15.338 (2)	15.299 (2)	15.283(2)	15.256(2)	15.2194 (19)	15.1945 (13)
β(º)	90.646(5)	90.531(7)	90.338 (2)	90.223 (2)	90.132(5)	90.103(9)	90.042 (2)	89.9200 (10)
V(Å^3)	3004.6(6)	2984.4(6)	2940.2 (7)	2925.7 (7)	2920.1(6)	2899.7(8)	2879.0 (6)	2867.3 (4)
Space group	C2/c	C2/c	C2/c	C2/c	C2/c	C2/c	C2/c	C2/c
Z	4	4	4	4	4	4	4	4
D_c(Mg•m^{-3})	2.169	2.199	2.259	2.278	2.306	2.330	2.363	2.384
μ(mm^{-1})	3.310	3.546	4.062	4.356	4.611	4.947	5.260	5.589
F(000)	1904	1912	1928	1936	1944	1952	1960	1968
T(K)	95(2)	95 (2)	100(2)	100(2)	95(2)	95(2)	100(2)	100(2)
θ_{max} (º)	36.6	36.7	31.8	32.0	36.8	32.3	31.9	32.1
Refln. Indep.	7065	7004	4681	4757	6894	4669	4671	4622
Refln. I>2σ(I).	6191	6250	4303	4572	5717	3682	4434	4320
R_{int}	0.0235	0.0222	0.0230	0.0180	0.030	0.0386	0.0210	0.0216
R1(I>2σ)	0.0241	0.0235	0.0215	0.0157	0.0282	0.0349	0.0162	0.0173
wR2(I>2σ)	0.0536	0.0542	0.0476	0.0383	0.0563	0.0662	0.0368	0.0385

Table 1 cont. Crystal Data and Summary of Data Collection and Refinement for $[Ln_2(TPNO_2)_3(H_2O)_2]\cdot 2H_2O$, Ln = Pr-Lu (except Pm)

$[Ln_2(TPNO_2)_3(H_2O)_2]\cdot 2H_2O$	Er	Tm	Yb	Lu
fw	1033.93	1037.26	1045.48	1049.34
a(Å)	16.678 (2)	16.662(2)	16.6258(15)	16.604 (3)
b(Å)	11.2891 (16)	11.2811(15)	11.2566(12)	11.231 (2)
c(Å)	15.182 (2)	15.172(2)	15.1513(15)	15.119 (3)
β(º)	89.8788 (18)	89.851(6)	89.762(5)	89.668 (3)
V($Å^3$)	2858.4 (7)	2851.8(6)	2835.5(5)	2819.5 (10)
Space group	C2/c	C2/c	C2/c	C2/c
Z	4	4	4	4
D_c($Mg\cdot m^{-3}$)	2.403	2.416	2.449	2.472
μ(mm^{-1})	5.942	6.292	6.667	7.074
F(000)	1976	1984	1992	2000
T(K)	100(2)	95(2)	95(2)	100(2)
θ_{max} (º)	30.5	34.9	38.4	31.9
Refln. Indep.	4268	5891	7599	4551
Refln. I>2σ(I).	3826	4473	6595	3615
R_{int}	0.0227	0.0400	0.0244	0.0502
R1(I>2σ)	0.0187	0.0334	0.0262	0.0342
wR2(I>2σ)	0.0369	0.0621	0.0596	0.0576

3. Results and Discussion

3.1. Synthesis

The reaction of the lanthanide(III) oxides (Ln_2O_3) with 2-nitroterephthalic acid (H_2TPNO_2) under hydrothermal conditions at 170˚C for 7 days produced water insoluble crystalline materials that formed up to millimeter-sized crystals. The crystal forms ranged from small, crystalline particles and rectangular blocks to decahedra. The formation of the $[Ln_2(TPNO_2)_3(H_2O)_2]\cdot 2H_2O$ frameworks seems to proceed via an acid-base reaction under hydrothermal conditions resulting in three-dimensional (3D) coordination polymers. In order to saturate the coordination sphere of the lanthanide(III) cations two water molecules coordinate to the metal centers per unit cell (one water molecule at each metal center). Two additional water molecules are taken up by the resulting lattice system within the interstices.

3.2. Solid State Structures

The lanthanide 2-nitroterephthalates crystallize in the monoclinic crystal system (space group *C*2/c) throughout the entire series from Pr – Lu (Pm not determined). The structural data at low temperatures (95 and 100K) show that all $[Ln_2(TPNO_2)_3(H_2O)_2]\cdot 2H_2O$ coordination polymers are isotypic. Recently Smith *et al.* reported the Sm, Eu, Gd, Tb, and Er analogues, of which they determined the single crystal XRD data for the Eu, Tb, and Er species.[22] To our knowledge the single crystal structures of the other frameworks in this series are reported here for the first time. While Smith *et al.* focus on the physicochemical properties of these networks; our work describes the structural trends within this extended series. Numerous trials synthesizing the cerium(III) analogue from Ce_2O_3 and H_2TPNO_2 resulted in the formation of a water soluble product, which we did not further characterize. To determine phase purity we performed powder

X-ray diffraction analyses (XRDs) on the bulk samples, which suggest that these coordination polymers crystallize in one phase as pure products. Only $[Tb_2(TPNO_2)_3(H_2O)_2]\cdot 2H_2O$ and $[Er_2(TPNO_2)_3(H_2O)_2]\cdot 2H_2O$ contained some metal oxide impurity, ca. 7 % of TbO_2 and 4.9 % of Er_2O_3. We attribute the small deviations in elemental analysis values found for the Tb- and Er-counterparts to these impurities. Figure 1 shows a Rietveld refinement plot for $[Nd_2(TPNO_2)_3(H_2O)_2]\cdot 2H_2O$, representative for all obtained products. (The data were refined against the corresponding single crystal X-ray data).

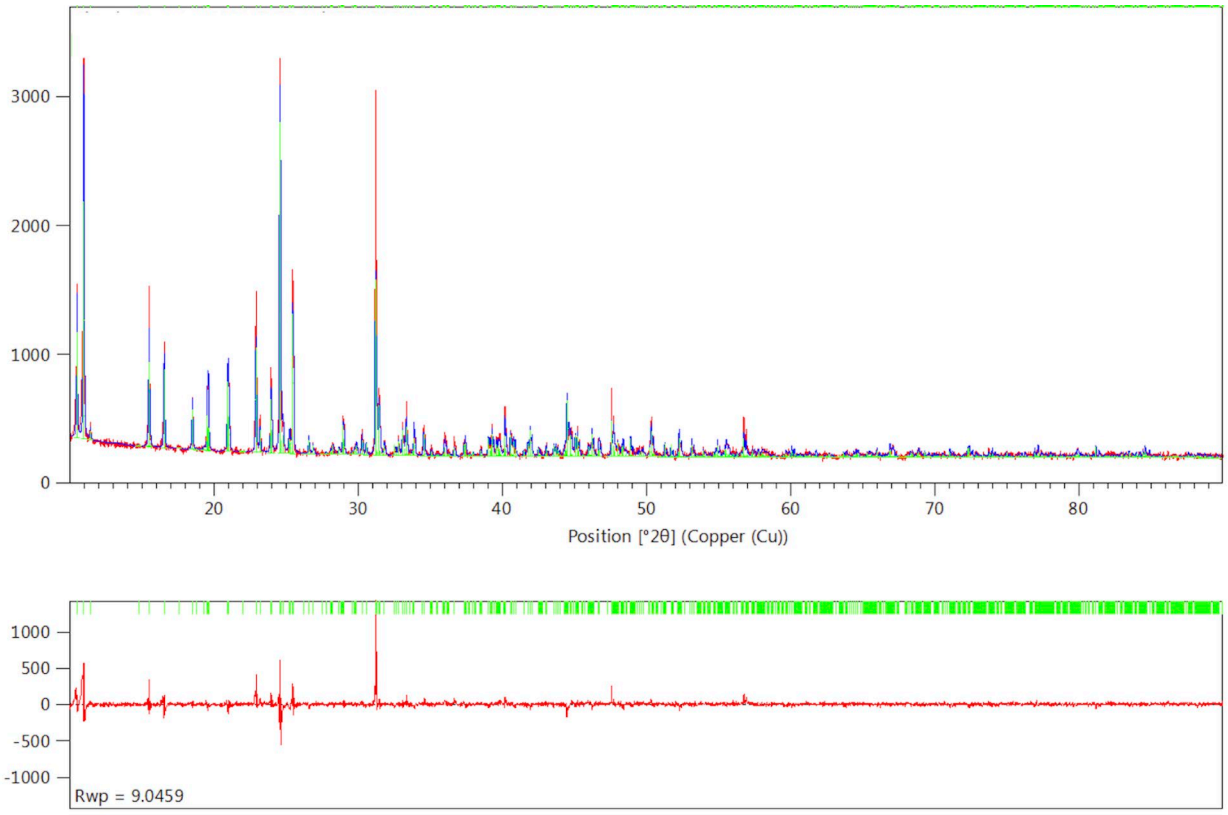

Figure 1. X-Ray Powder Diffraction pattern for $[Nd_2(TPNO_2)_3(H_2O)_2]\cdot 2H_2O$, representative for all lanthanide 2-nitroterephthalates reported herein (other plots are given in the SI). Top: Black trace: experimental pattern, red trace Rietveld fit calculated based on the single crystal data for $[Nd_2(TPNO_2)_3(H_2O)_2]\cdot 2H_2O$. Bottom: Difference plot. The agreement of calculated and experimental XRD peaks suggests that the samples were phase pure.

The oxidation of Tb^{3+} to Tb^{4+} in the detected impurity is particularly unexpected as no attempt was made to add any oxidizing agent to the reaction mixture besides the starting materials.

All $[Ln_2(TPNO_2)_3(H_2O)_2]\cdot 2H_2O$ networks in this series are isomorphous and arrange in identical extended 3D-lattice structures. All structures exhibit identical $[Ln_2(TPNO_2)_3(H_2O)_2]\cdot 2H_2O$ units, in which each lanthanide center is coordinated to 8 surrounding oxygen atoms. Throughout the series the unit cell parameters, including the angle β and the cell volume, consistently show a gradual decrease when plotted versus the ionic radius of the corresponding Ln(III) ions. The Ln-O bond distances for corresponding LnO_8 polyhedra exhibit the same trend and range from 2.215 Å to 2.67Å.

We will discuss the structural details of all networks using the $[Nd_2(TPNO_2)_3(H_2O)_2]\cdot 2H_2O$ species for representative purposes. These isomorphous coordination networks incorporate one crystallographic type of Ln(III) ion respectively, and form layers of neighboring metal centers that are linked together along the *c*-axis by the carboxylate groups of 2-nitroterephthalate ($TPNO_2$) entities.

Eight O-atoms coordinate to the lanthanide centers, of which seven are part of the terephthalate carboxylates and one stems from a water molecule. The resulting LnO_8-coordination-polyhedra are comprised of distorted trigonal prisms, of which two faces are capped with semi octahedra. Thus, with this structural motif of the LnO_8 coordination spheres, these structures are related to the $PuBr_3$ structure type.[23]

Figure 2 illustrates the highly linked 3D-network of 2-nitroterephthalate entities and Ln-centers with view onto the *ac*-plane. One important aspect is that this network incorporates two different types of $TPNO_2$ entities:

$TPNO_2$-linkers running down the *b*-axis exhibit disorder of the nitro group and we marked them with orange nitro-group oxygen atoms in illustrations and assigned the abbreviation **$TPNO_2$-1**. The other type of 2-nitroterephthalate linkers tie together the *bc*-layers in direction *a*, while stretching diagonal across the *ac*-plane. These spacers, connecting *bc*-layers in direction *a*, do not show disorder and are marked with purple nitro-group oxygen atoms in illustrations, while being assigned the abbreviation **$TPNO_2$-2**.

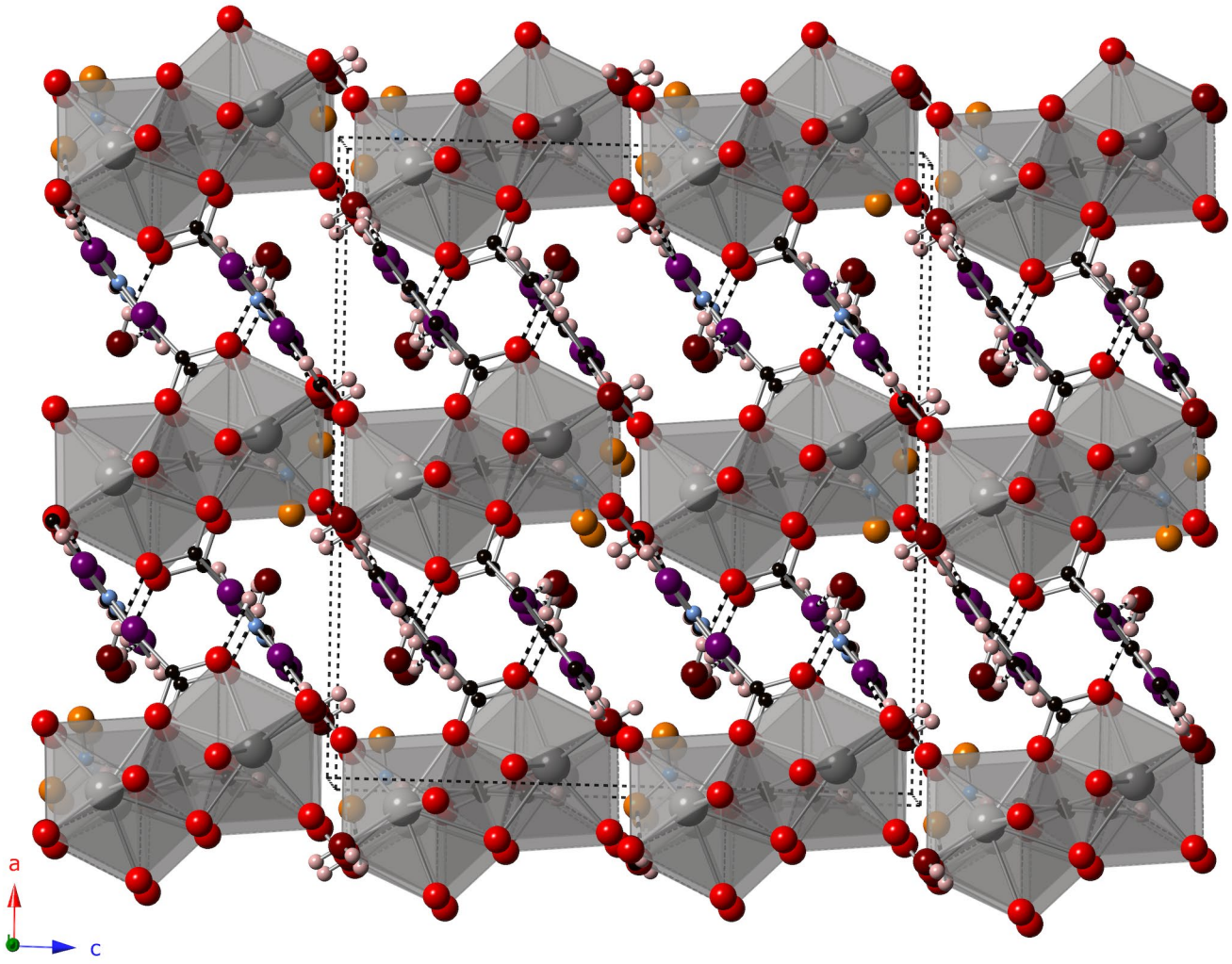

Figure 2. View onto the *ac*-plane of monoclinic $[Nd_2(TPNO_2)_3(H_2O)_2]\cdot 2H_2O$ illustrating the layers, aligned with the *c*-axis, being tied together in direction *a* by **$TPNO_2$-2**. Ln_2O_{14}-clusters assemble via edge-sharing from individual LnO_8-coordination polyhedra, whose structural motif can most closely be portrayed as a distorted bicapped trigonal prism. Edge-sharing is facilitated by two μ-coordinating carboxylate O-atoms (O4) stemming from respectively one **$TPNO_2$-2** on each side of the layer (grey = Nd, orange = O (from NO_2 groups belonging to

TPNO$_2$-1 spacers stretching along *b*-axis), purple = O (from NO_2 groups belonging to **TPNO$_2$-2** linkers aligning diagonal to the *ac*-plane), red = O (from carboxylate units), maroon = O (from H_2O), white = H). One can also recognize the coordinating water molecules that are positioned at the opposite tips of the Ln_2O_{14}-clusters engaging in hydrogen-bonding towards **TPNO$_2$-2** nitro groups as well as to interstitial water molecules, which on their part further connect to **TPNO$_2$-2** nitro groups via hydrogen bonds.

The 3D-network is segmented into layers of LnO_8-coordination-polyhedra throughout the *bc*-plane assembling as Ln_2O_{14}-clusters via edge-sharing through two carboxylate oxygen atoms. Both of these O-atoms bridge the two Ln-metal centers and stem from two 2-nitroterephthalate spacers (**TPNO$_2$-2**), of which one is positioned on each side of the *bc*-layer respectively. Furthermore, these two oxygen atoms occupy the respective tip of one semi-octahedron belonging to each Ln-central atom. The other semi-octahedron tip is occupied by the coordinating water molecule of each LnO_8-coordination polyhedron respectively. Thus each Ln_2O_{14}-cluster possesses a pointed tip on both ends populated with coordinating water molecules. The coordinated H_2O-molecules connect via hydrogen bonds to one **TPNO$_2$-2** nitro group (purple O-atoms) and to one of the interstitial water molecules, which are further held in place via hydrogen bonds to two **TPNO$_2$-2** nitro groups respectively.

Each end of the Ln_2O_{14}-clusters is interlinked along the *c*-axis through two carboxylate groups, stemming from **TPNO$_2$-2** entities rendering them as zig/zag chains in *c*-direction as shown in Figure 3.

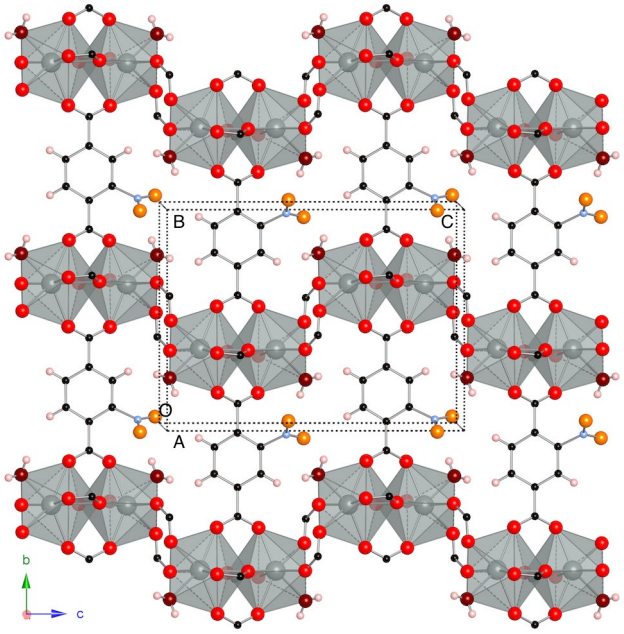

Figure 3. Buildup of the *bc*-layer via linkage of Ln_2O_{14}-clusters by 2-nitoterephthalate units (grey = Nd, orange = O (from NO_2 groups belonging to **TPNO₂-1** stretching along *b*-axis), red = O (from carboxylate units), maroon = O (from H_2O), white = H). Infinite zig/zag chains of Ln_2O_{14}-polyhedra in *c*-direction result through linkage via two carboxylate groups on each end, also originating from one **TPNO₂-2** on each side of the layer. Individual zig/zag chains are tied together along the *b*-axis by **TPNO₂-1** linkers.

These carboxylate functional groups are provided by **TPNO₂-2** linkers that sit on opposite sides of the corresponding *bc*-layer and tie these layers together in *a*-direction (Figure 1). These carboxylates serve as bridging entities, whose oxygen atoms coordinate in a mono-dentate fashion to the two metal centers. Consequently, each **TPNO₂-2** spacer delivers one carboxylate group that provides edge-sharing O-atoms (O4), assisting LnO_8-polyhedra with the assemblance as Ln_2O_{14}-clusters on one side. This COO^--entity chelates one of the cluster's Ln^{3+} ion, while the edge sharing O(4)-atom of that carboxylate bridges both Ln^{3+}-ions μ-fashion. The carboxylate group on the other side interlinks Ln_2O_{14}-clusters via κ^1-bridging. Figure 2 further illustrates the linkage of the above described zig/zag chains in *b*-direction by the **TPNO₂-1** linkers. Individual Ln_2O_{14}-clusters stack on top of each other, separated by **TPNO₂-1** units, forming infinite straight columns along the *b*-axis. This demonstrates the build up of individual layers in the *bc*-plane.

Smith *et al.* determined the topology of these structures to be a 4,4,6-c net with point symbol {4^2.6^4}{4^3.6^3}2{4^8.6^6.8}2.[22]

Torsion angles between the **TPNO$_2$-1** carboxylate groups and the aromatic rings range between 17.4° - 26.6° for the Pr-compond and between 18.4° - 24.9° for the Lu-species. The ones for **TPNO$_2$-2** are between 4.5° - 96.5° (Pr) and 9.3° - 96.0° (Lu). These are mild fluctuations on torsion angles between individual Ln-species and we cannot observe any linear trend along the series. Thus, the torsion angles do not allow any conclusions with regard to how the crystal lattice is dealing with strain build up along the series. The small out of plane torsion of the **TPNO$_2$-1** units suggest that these frameworks may potentially possess electronic properties that would allow for electronic communication between metal centers along the *b*-axis as conjugate systems of aromatic spacers are intact (Figure 3), whereas a comlete disruption of the conjugate system, diagonally segmenting the *ac*-plane, results for the **TPNO$_2$-2** units (Figure 4).

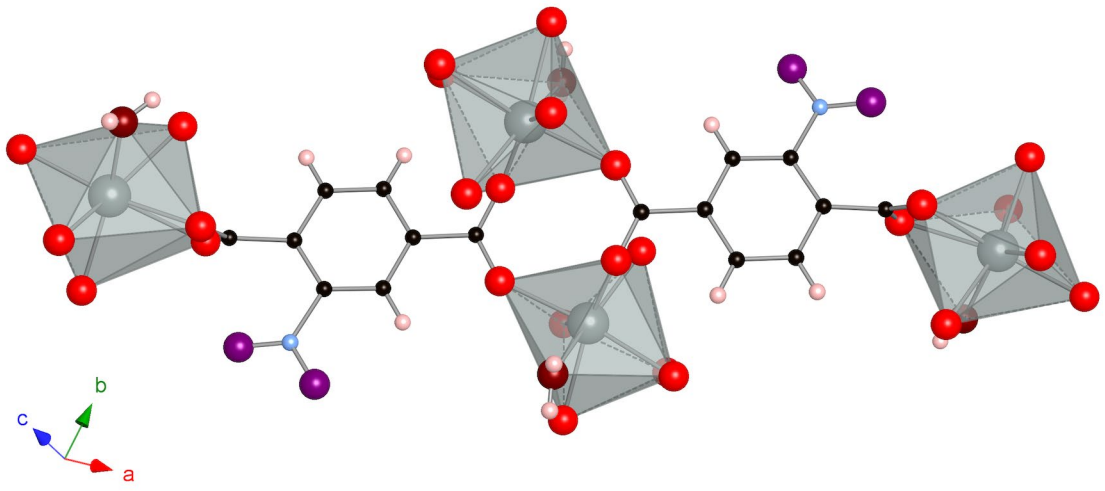

Figure 4. A string of **TPNO$_2$-2** entities crossing the *ac*-plane (grey = Nd, purple = O (from NO_2 groups belonging to **TPNO$_2$-2** linkers, red = O (from carboxylate units), maroon = O (from H_2O), white = H). In the center both carboxylate groups coordinate in a bridging bidentate fashion to two separate LnO_8 polyhedra with torsion angles of 5.0° and 6.1°. On the other side carboxylate groups chelate to an LnO_8 polyhedron, while also coordinating to the

adjacent LnO_8 polyhedron of that Ln_2O_{14} cluster. As a result, those carboxylate groups are twisted out of the aromatic planes by more than 95°, completely disrupting the conjugate system for the **$TPNO_2$-2** units.

The angle β as well as the unit cell volume plotted versus the ionic radius clearly suggest that this system does not experience any significant strain build up. Figure 5 illustrates that both parameters decline gradually with decreasing ionic radii. This and the fact that there is no structural rearrangement along this series is in stark contrast as to what we previously observed for the lanthanide bis-hydroxychlorides and the lanthanide hydroxysulfates. The lanthanide bis-hydroxychlorides also crystallize in an 8-coordinate structural arrangement along the entire series, however, a non-gradual segment in unit cell volume plotted versus ionic radius indicates that there seems to be a significant amount of stress buildup between Tb and Tm.[8]

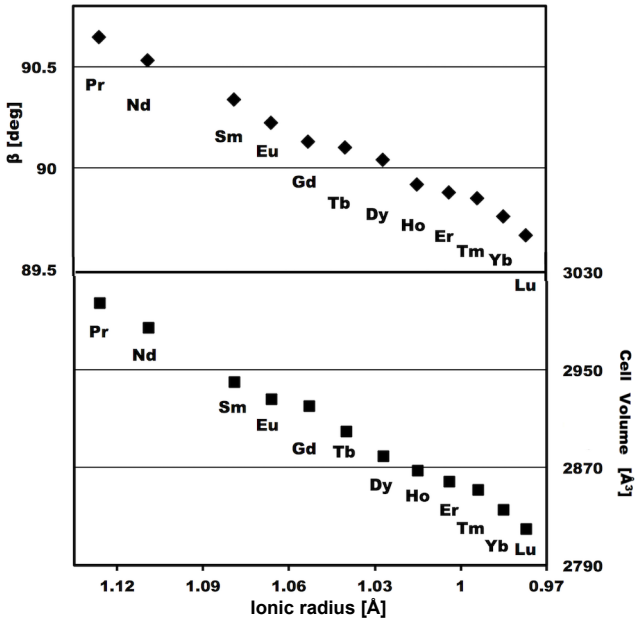

Figure 5. Unit cell volume and angle-β in correlation with trivalent lanthanide(III) ionic radius (Å).[24]

For the lanthanide hydroxysulfates we see a structural rearrangement with a change from coordination number 8 to 9 between Gd and Tb. The plot of the unit cell volume versus ionic

radius here shows that between the isomorphous 9-coordinate $Ln(OH)SO_4$ (Pr – Gd) as well as the also isomorphous 8-coordinate $Ln(OH)SO_4$ between Tb and Lu that there is no significant strain buildup within the individual sections of $Ln(OH)SO_4$ respectively.[9] The unit cell parameters, a, b, and c, show gradual declines going along with decreasing ionic radius throughout the series of $[Ln_2(TPNO_2)_3(H_2O)_2]\cdot 2H_2O$, corroborating that there seems to be no noticeable stress affecting the crystal lattice within this series. While the networks containing small rigid inorganic anions deal with a strain buildup one way or the other, any amounting strain in the $[Ln_2(TPNO_2)_3(H_2O)_2]\cdot 2H_2O$ seems to be compensated by the more flexible and much more spacious 2-nitroterephthalate linkers via out of plane torsion. Figure 6a shows that the same trend can be observed for the individual Ln-O bond lengths of the LnO_8 coordination polyhedra.

Table 2. Ln-O bond lengths for LnO_8 coordination polyhedra. All values are in Ångström (Å).

LnO_8	Ln-O1 (κ^1)	Ln-O2 (κ^1)	Ln-O3 (κ^1)	Ln-O4 (μ)	Ln-O4 (μ) second	Ln-O11 (terminal H_2O)	Ln-O7 (κ^1)	Ln-O8 (κ^1)
Pr	2.4037 (12)	2.3767 (13)	2.5530 (13)	2.4374 (13)	2.6717 (13)	2.4548 (14)	2.4122 (13)	2.4592 (13)
Nd	2.3913 (12)	2.3589 (12)	2.5353 (13)	2.4143 (13)	2.6505 (12)	2.4379 (14)	2.3976 (13)	2.4496 (13)
Sm	2.3603 (14)	2.3260 (16)	2.5045 (16)	2.3861 (15)	2.6155 (15)	2.4061 (16)	2.3629 (15)	2.4159 (15)
Eu	2.3487 (11)	2.3107 (12)	2.4897 (12)	2.3716 (12)	2.6028 (12)	2.3951 (13)	2.3546 (12)	2.4076 (12)
Gd	2.3409 (16)	2.3015 (16)	2.4804 (17)	2.3680 (16)	2.5898 (17)	2.3843 (18)	2.3439 (16)	2.4003 (16)
Tb	2.326 (3)	2.287 (3)	2.465 (3)	2.348 (3)	2.579 (3)	2.369 (3)	2.331 (3)	2.383 (3)
Dy	2.3085 (13)	2.2720 (13)	2.4517 (14)	2.3354 (14)	2.5647 (14)	2.3554 (14)	2.3122 (13)	2.3716 (13)
Ho	2.2998 (14)	2.2598 (14)	2.4349 (14)	2.3263 (14)	2.5534 (14)	2.3443 (16)	2.3006 (14)	2.3630 (14)
Er	2.2900 (16)	2.2508 (16)	2.4231 (17)	2.3146 (17)	2.5510 (16)	2.3328 (18)	2.2899 (16)	2.3522 (16)
Tm	2.281 (2)	2.238 (2)	2.415 (2)	2.305 (2)	2.537 (2)	2.322 (3)	2.284 (2)	2.349 (2)
Yb	2.2666 (16)	2.2263 (16)	2.4022 (17)	2.2909 (17)	2.5339 (17)	2.3138 (18)	2.2650 (16)	2.3302 (16)
Lu	2.258 (3)	2.215 (3)	2.392 (3)	2.282 (3)	2.524 (3)	2.300 (4)	2.253 (3)	2.321 (3)

Table 3. Various important distances. All values are in Ångström (Å).

Ln	Ln-Ln (within Ln_2O_{14} clusters)	Ln-Ln (between Ln_2O_{14} clusters)	O---H (shortest hydrogen bonds) H11A-O12, H12B-O3, H12A-O5, H11B-O6
Pr	4.097	5.254	1.830, 1.951, 2.115, 2.167
Nd	4.068	5.251	1.818, 1.925, 2.106, 2.194
Sm	4.019	5.242	1.821, 1.941, 2.054, 2.164
Eu	3.999	5.228	1.806, 1.940, 2.034, 2.168
Gd	3.984	5.221	1.811, 1.962, 2.130, 2.182
Tb	3.968	5.222	1.794, 1.958, 2.105, 2.207
Dy	3.947	5.204	1.806, 1.944, 2.009, 2.169
Ho	3.936	5.197	1.812, 1.928, 2.075, 2.162
Er	3.925	5.193	1.828, 1.947, 1.988, 2.212
Tm	3.915	5.205	1.818, 1.953, 2.115, 2.222
Yb	3.901	5.179	1.816, 1.983, 2.034, 2.211
Lu	3.890	5.172	1.816, 2.041, 2.117, 2.254

These trends further confirm that this system seems to adapt smoothly to smaller ionic radii without noticeable stress impacting the crystal lattice. The bond length values are tabulated in Table 2. Figure 6b showcases the immediate coordination environment around Ln(III) centers for the Nd-coordination polymer. Complementing Figure 6a, we used the same color codes for O-atoms corresponding to the respective Ln-O bonds. The two Ln(III) centers are linked through both O(4) atoms (light blue) in μ-fashion resulting in an $Ln_2O(4)_2$-ring. This arrangement facilitates the edge sharing of adjacent LnO_8 polyhedra to assemble as Ln_2O_{14} clusters. The Ln-O(3) bond is terminal and chelating (pink). Ln-O(7) and Ln-O(8) bonds (red and dark blue) belong to **$TPNO_2$-1** carboxylates, which are bridging and chelating between two adjacent Ln(III) centers, resulting in $Ln_2O_4C_2$-rings within Ln_2O_{14}-clusters. The Ln_2O_2- and $Ln_2O_4C_2$-rings are nearly orthogonal to one another. Ln-O(1) and Ln-O(2) (yellow and green) belong to **$TPNO_2$-2** carboxylates that serve as bridges between Ln_2O_{14}-clusters. Thus, this results in a second type of $Ln_2O_4C_2$-ring, interlinking Ln_2O_{14}-clusters. The Ln-O(11) bond (maroon) originates from terminal water molecules.

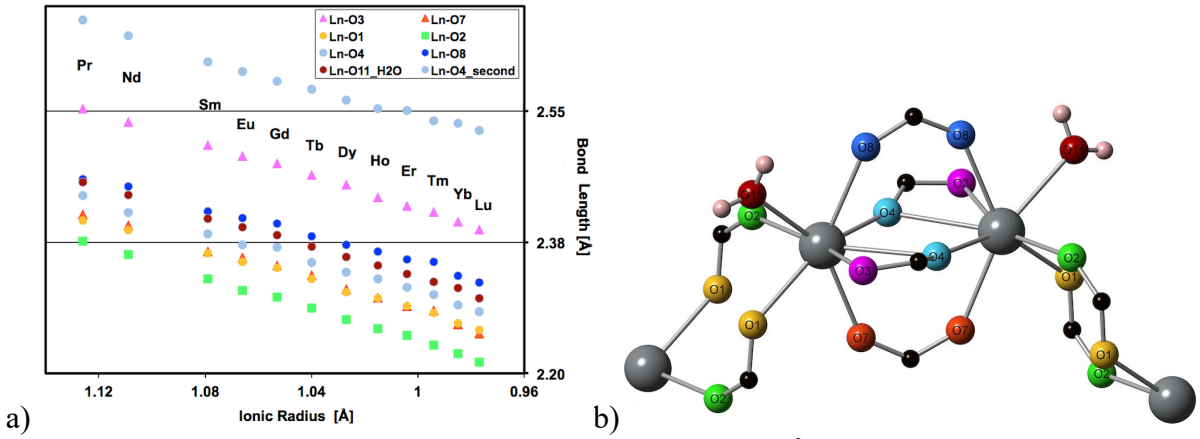

Figure 6. **a)** Ln-O bond lengths of LnO_8 polyhedra vs. Ln^{3+} ionic radius (Å).[24] **b)** Coordination environment around two linked Nd-central atoms with the same color coding of the corresponding Ln-O distances in **a)**.

In Table 3 we list the Ln-Ln distances within Ln_2O_{14} clusters as well as between clusters.

We also show the four shortest hydrogen bond lengths, which represent the connection of interstitial H_2O to coordinating H_2O (H(11A)-O(12)), interstitial water to the coordination polyhedra and nitro groups (H(12B)-O(3), H(12A)-O(5)), as well as coordinating water to nitro groups (H(11B)-O(6)).

3.3. Thermogravimetric analysis.

All samples were subjected to thermogravimetric analysis in order to examine the thermal stabilities of the lanthanide 2-nitroterephthalates. The first loss of mass for all products, between 110 - 190˚C corresponds to the loss of the interstitial water, which is held in place via hydrogen bonds between a nitro-oxygen atom of **$TPNO_2$-2**, a carboxylate oxygen atom, as well as a coordinating water molecule. The second loss of mass is detected between 200 and 340˚C, corresponding to the loss of the coordinated water molecules. Both of these mass reductions relate to a step of 3.4-4.0% (theoretically calculated 3.4-3.7%). Between 330 and 440˚C we detected the degradation of one $TPNO_2$ entity, which corresponds to a mass reduction of 18.4-20.6% (calculated 18.4-19.7%). The final step in the TGA curves indicated the loss of two $TPNO_2$-units starting at 440˚C and leveling off before 900˚C, with a mass loss of 35.4 - 40.0% (calculated 36.8 - 39.4%). The spacers in each Ln-coordination polymer leave behind an oxygen atom to produce the final Ln(III) oxide (Ln_2O_3). The Er-analogue showed a significantly different weight loss for the removal of the linkers (56.67%), which corroborates the observations Smith *et. al* made for this compound.[22] It seems that while all other networks form the corresponding Ln(III) oxides, the Er-species forms erbium(III) oxalate, $Er_2(C_2O_4)_3$, as the residue after thermal decomposition.

The temperatures representing the loss of coordinated water molecules show a gradual increase (Figure 7) with the decline of ionic radius, corroborating the other data. Due to the decreasing size of the coordination polyhedra towards the heavier lanthanide elements, the coordination bonds of these water molecules are reduced in length, resulting in the strengthening of the interactions between water molecules and Ln^{3+} -ions. The removal temperatures of the interstitial water molecules did not show a similar trend, indicating little to no dependence upon the identity of the Ln^{3+} ion. The temperatures we measured for the interstitial water molecules to be driven out are lower than what Smith *et al.* reported for theirs (~60˚C lower for the Eu-species).[22] According to our measurements the loss of coordinated water also occurred at slightly lower temperatures compared to their experiment. This discrepancy is easily accounted for by experimental conditions. Faster heating rates regularly shift mass loss events to slightly higher temperatures. In the previous report, Smith *et al.* used a heating rate of 15˚C/min., whereas we used 10˚C /min.

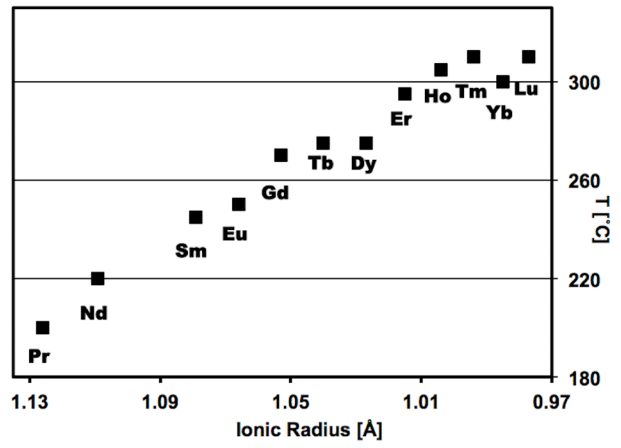

Figure 7. Temperature for the removal of coordinated water vs. Ln^{3+} radius (Å).[24]

3.4. Vibrational data

All $[Ln_2(TPNO_2)_3(H_2O)_2]\cdot 2H_2O$ networks were characterized by FT-IR spectroscopy and all spectra look alike with minor fluctuations of specific peaks along the series. None of these peaks show any trends along the series, therefore we illustrate the FT-IR spectrum of $[Tb_2(TPNO_2)_3(H_2O)_2]\cdot 2H_2O$ to represent all IR spectra in Figure 7. Peaks between 3600 and 3300 cm^{-1} stem from coordinating as well as interstitial water, representing the stretching modes ν_s = 3600 - 3588 and ν_{as} = 3510 - 3470 cm^{-1}. Water's deformation mode is also visible between 1635 and 1625 cm^{-1}. We measured the vibrational spectra of all products previously dried at room temperature, at 105˚C, and 170˚C. No significant differences between spectra, dried at these temperatures, can be observed. This nicely complements the data of the TGA measurements, showing that coordinating water is not driven out below 200˚C.

The IR stretching frequencies of the carboxylate groups (ν C-O) are found between 1590 cm^{-1} and 1580 cm^{-1} for ν_{as}, and between 1411 cm^{-1} and 1405 cm^{-1} for ν_s. The average Δ-value of 176 cm^{-1} confirms the syn syn bidentate bridging between two Ln^{3+}-centers by both carboxylate entities in **$TPNO_2$-1**, as well as on one side of **$TPNO_2$-2**. The chelation of Ln^{3+} on the opposite side of **$TPNO_2$-2** and the simultaneous coordination to the Ln^{3+} of the adjacent LnO_8 polyhedron of this Ln_2O_{14} cluster affords peaks for ν_{as}, between 1555 cm^{-1} and 1535 cm^{-1} as well as for ν_s between 1390 cm^{-1} and 1379 cm^{-1} as described in detail by Deacon *et al.*[25] and Bakalbassis *et al.*[26] These vibrational values confirm the structural details as observed for the coordination of the carboxylates in the single crystal X-ray structures. The hydrogen atoms attached to the aromatic rings show bands between 3100 and 3000 cm^{-1}. The values for ν_{as} (N-O), of the nitro group are found near 1500 cm^{-1} and the symmetric N-O stretches lie between 1340 and 1350 cm^{-1}. In Table 4 we list the most important IR-frequencies for the coordination polymers.

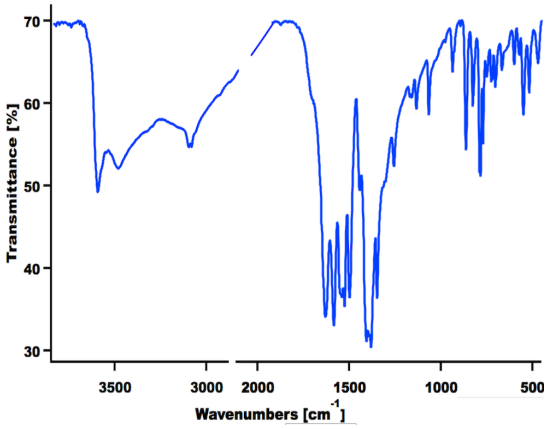

Figure 8. IR spectrum of $[Tb_2(TPNO_2)_3(H_2O)_2]\cdot 2H_2O$ representative for all networks (dried at room temperature).

Table 4. Vibrational data for $[Ln_2(TPNO_2)_3(H_2O)_2]\cdot 2H_2O$, Ln = Pr-Lu (except Pm). All values are in wavenumbers (cm^{-1}).

$[Ln_2(TPNO_2)_3(H_2O)_2]\cdot 2H_2O$	Pr	Nd	Sm	Eu	Gd	Tb	Dy	Ho	Er	Tm	Yb	Lu
ν_s O-H (H_2O)	3597	3599	3589	3588	3593	3593	3593	3593	3593	3593	3595	3596
ν_{as} O-H (H_2O)	3470	3505	3469	3481	3482	3483	3483	3495	3488	3502	3506	3502
δ O-H (H_2O)	1628	1626	1628	1628	1627	1632	1634	1632	1634	1634	1635	1636
ν C-H	3096 3081	3096 3081	3097 3080	3097 3079	3097 3081	3098 3080	3098 3082	3098 3080	3098 3082	3098 3082	3098 3083	3100 3083
ν_s C-O (COO-Ln bridging)	1406	1406	1406	1411	1409	1406	1409	1408	1411	1411	1408	1411
ν_{as} C-O (COO-Ln bridging)	1580	1584	1581	1581	1586	1585	1585	1582	1587	1587	1587	1586
Δ-value	174	178	175	170	177	179	176	174	176	176	179	175
ν_s C-O (COO-Ln chelating (κ^2))	1390	1393	1379	1394	1394	1393	1381	1383	1383	1384	1384	1380
ν_{as} C-O (COO-Ln chelating (κ^2))	1546	1545	1546	1535	1545	1540	1550	1550	1550	1553	1553	1543
Δ-value	156	152	167	141	151	134	169	167	167	169	169	163
ν_s N-O	1343	1345	1348	1348	1348	1348	1348	1348	1348	1348	1348	1349
ν_{as} N-O	1497	1497	1491	1497	1497	1499	1495	1499	1499	1499	1499	1501

Conclusions

Using hydrothermal syntheses we created a series of isomorphous $[Ln_2(TPNO_2)_3(H_2O)_2]\cdot 2H_2O$ coordination polymers at 170˚C. This series includes the lanthanide elements Pr through Lu, with the exception of Pm. The Ln^{3+} ions are surrounded by 8 coordinating oxygen atoms, creating LnO_8 coordination polyhedra that are interlinked by 2-nitroterephthalate as well as bridging carboxylate groups, resulting in a 3D coordination network. The structural properties are represented by a gradual decrease of unit cell parameters a, b, c, β, of the individual Ln-O bond lengths of LnO_8 coordination spheres, as well as of the unit cell volume versus the decreasing ionic radius along the series. This indicates a smooth crystal lattice adaption to smaller ionic radii and bond lengths without any significant strain buildup. Unlike observed in our other investigations, where small rigid inorganic anions lacked the ability to alleviate substantial strain buildup, the 2-nitroterephthalate spacers in this series seem to allow for more flexibility, and thus, the lattice parameters indicate that there is hardly any stress impact on the crystal lattice while adjusting to smaller ionic radii. Powder diffraction studies confirm that individual products were obtained in high purities with minor remains of lanthanide oxide starting materials for the Tb and Er counterparts. Thermogravimetric data show that coordinating water molecules leave the coordination sphere with gradually increasing temperatures between 190 and 310˚C. This corroborates the X-ray data, which show that Ln-O bond lengths are gradually decreasing with no substantial irregularities with increasing atomic numbers of individual lanthanide elements. The FT-IR spectra corroborate the structural properties with regard to the coordination of carboxylate groups towards Ln^{3+} ions and the role that these functional groups play, considering the bridging of LnO_8 polyhedra and Ln_2O_{14} clusters.

While our previous investigations of $Ln(OH)_2Cl$ and $Ln(OH)SO_4$ series revealed complicated associations between individual unit cell parameters and corresponding ionic radii, the trends observed for the $[Ln_2(TPNO_2)_3(H_2O)_2]\cdot 2H_2O$ species can be viewed as more straightforward, which we attribute to the added flexibility of the 2-nitroterephthalate linkers.

Acknowledgments

This work was supported at the University of Louisiana at Monroe by the Department of Chemistry. We would like to thank the Louisiana Board of Regents for the sponsorship of this research under contract#: LEQSF(2007-10)-RD-A-40. Financial support at Angelo State University was awarded by the Department of Chemistry & Biochemistry, through university startup funds, the Welch Foundation, and the faculty research enhancement program (FREP). Funding for the X-ray diffractometer at Youngstown State University was provided by NSF Grant 0087210, Ohio Board of Regents Grant CAP-491, and by Youngstown State University. The purchase of the X-ray diffractometer at Louisiana State University was made possible by Grant No. LEQSF(1999-2000)-ENH-TR-13, administered by the Louisiana Board of Regents. TGA experiments were funded through university startup funds from Florida Atlantic University.

Appendix A. Supplementary data

Powder XRD data, table with bond lengths, and TGA curves. Single crystal X-ray data have been deposited with the Cambridge Crystallographic Data Centre with Nos. 1549877-1549888. Copies of the data can be obtained free of charge via the Internet at: https://www.ccdc.cam.ac.uk/structures/

References

[1] (a) H. Giesber, J. Ballato, G. Chumanov, J. Kolis, M. Dejneka, J. Appl. Phys., 93 (2003) 8987-8994;
(b) J.M. Haschke, in: K.A. Gschneidner, Jr., L. Eyring (Eds.) Handb. Phys. Chem. Rare Earths, North-Holland Publishing Company, 1979, pp. 89-151;
(c) N. Kaltsoyannis, The f elements, Oxford University Press, Oxford, New York, 1999;
(d) M.S. Wickleder, Chem. Rev., 102 (2002) 2011-2087;
(e) M. Seitz, M.D. Pluth, K.N. Raymond, Inorg . Chem., 46 (2007) 351-353;
(f) M. Seitz, A.G. Oliver, K.N. Raymond, J. Am. Chem. Soc., 129 (2007) 11153-11160.

[2] H. Giesber, J. Ballato, W. Pennington, J. Kolis, Inform. Sciences, 149 (2003) 61-68.

[3] (a) Z. Amghouz, S. Garcia-Granda, J.R. Garcia, R.A. Ferreira, L. Mafra, L.D. Carlos, J. Rocha, Inorg. Chem., 51 (2012) 1703-1716;
(b) C. Daiguebonne, N. Kerbellec, K. Bernot, Y. Gerault, A. Deluzet, O. Guillou, Inorg. Chem., 45 (2006) 5399 - 5406;
(c) C. Daiguebonne, N. Kerbellec, O. Guillou, J. Bünzli, C.;, F. Gumy, L. Catala, T. Mallah, N. Audebrand, Y. Gérault, K. Bernot, G. Calvez, Inorg. Chem., 47 (2008) 3700 - 3708;
(d) A. Deluzet, W. Maudez, C. Daiguebonne, O. Guillou, Cryst. Growth Des., 3 (2003) 475 - 479; (e) L. Pan, N. Zheng, Y.M. Wu, S. Han, R. Yang, X. Huang, J. Li, Inorg. Chem., 40 (2001) 828 - 830; (f) T. Reinecke, M. Eddaoudi, M. Fehr, D. Kelly, O.M. Yaghi, J. Am. Chem. Soc., 121 (1999) 1651-1657;
(g) R.A. Zehnder, R.A. Renn, E. Pippin, M. Zeller, K.A. Wheeler, J.A. Carr, N. Fontaine, N.C. McMullen, J. Molec. Struct., 985 (2011) 109-119;
(h) S. Freslon, Y. Luo, C. Daiguebonne, G. Calvez, K. Bernot, O. Guillou, Inorg. Chem., 55 (2016) 794-802.

[4] (a) G.D. Del Cul, S.E. Nave, G.M. Begun, J.R. Peterson, . J. Raman Spectrosc., 23 (1992) 267-272;
(b) G.D. Del Cul, S.E. Nave, J.R. Peterson, J. Alloy. Compd., 193 (1993) 194-196;
(c) D.K. Fujita, B.B. Cunningham, T.C. Parsons, Inorg. Nucl. Chem. Lett., 5 (1969) 307-313;
(d) J.R. Peterson, Nucl. Sci. Abstr., 22 (1968) 6292;
(e) J.R. Peterson, B.B. Cunningham, J. Inorg. and Nucl. Chem., 30 (1968) 823-828;
(f) T.M. Schleid, L.R.; Meyer, G., J. Less-Common Met., 127 (1987) 183-187;
(g) D.H. Templeton, C.H. Dauben, J. Am. Chem. Soc., 75 (1953) 4560-4562.

[5] (a) B. Chen, Y. Yang, F. Zapata, G. Lin, G. Qian, E.B. Lobkovsky, Adv. Mater., 19 (2007) 1693-1696;
(b) A. de Bettencourt-Dias, P.S. Barber, S. Bauer, J. Am. Chem. Soc., 134 (2012) 6987-6994;
(c) C. Feldmann, T. Jüstel, C.R. Ronda, P.J. Schmidt, Adv. Funct. Mater., 13 (2003) 511-516;
(d) T. Jüstel, H. Nikol, C. Ronda, Angew. Chem. Int. Ed., 37 (1998) 3084-3103;
(e) S. Kuck, Appl. Phys. B: Laser Opt., 72 (2001) 515;
(f) H. Yokoyama, Science, 256 (1992);
(g) D.T. De Lill, N.S. Gunning, C.L. Cahill, Inorg. Chem., 44 (2005) 258-266.

[6] (a) X. Li, M.Q. Zha, X.W. Wang, R. Cao, Inorg. Chim. Acta 362 (2009) 3357–3363;
(b) C.G. Wang, Y.H. Xing, Z.P. Li, J. Li, X.Q. Zeng, M.F. Ge, S.Y. Niu, J. Mol. Struct., 921 (2009) 126–131;
(c) X.W. Wang, X. Li, J.Z. Chen, G. Zheng, H.L. Hong, Eur. J. Inorg. Chem., (2008) 98–105;
(d) R.B. Luebke, Y., L.J. Weselinski, A.J. Cairns, M. Alkordi, G. Norton, L.A. Wojtas, K., M. Eddaoudi, Chem. Sci., 6 (2015) 4095–4102;
(e) D.X. Xue, Y. Belmabkhout, O. Shekhah, H. Jiang, K. Adil, A.J. Cairns, M. Eddaoudi, J. Am. Chem. Soc., 137 (2015) 5034-5040;
(f) S.N. Zhao, L.J. Li, X.Z. Song, M. Zhu, Z.M. Hao, X. Meng, L.L. Wu, J. Feng, S.Y. Song, C. Wang, H.J. Zhang, Adv. Funct. Mater., 25 (2015) 1463-1469.

[7] (a) M.B. Andrews, C.L. Cahill, Chem. Rev., (2012);
(b) P. Burns, C., Y. Ikeda, K. Czerwinski, Am. Bullet, 35 (2010) 868-876;
(c) J.L. Crandall, Scient. Basis Nucl. Waste Mgmt., 2 (1980) 39-51;
(d) R.C. Ewing, Can. Mineral., 39 (2001) 697 - 715;
(e) S.K. Ghose, Y. Li, A. Yakovenko, E. Dooryhee, L. Ehm, L.E. Ecker, A.-C. Dippel, G.J. Halder, D.M. Strachan, P.K. Thallapally, J. P. Chem. Lett., 6 (2015) 1790-1794.

[8] R.A. Zehnder, D.L. Clark, B.L. Scott, R.J. Donohoe, P.D. Palmer, W.H. Runde, D.E. Hobart, Inorg. Chem., 49 (2010) 4781-4790.

[9] R.A. Zehnder, C.S. Wilson, H.T. Christy, K.S. Harris, V. Chauhan, V. Schutz, M. Sullivan, M. Zeller, F.R. Fronczek, J.A. Myers, K. Dammann, J. Duck, P.M. Smith, A. Okuma, K. Johnson, R. Sovesky, C. Stroudt, R.A. Renn, Inorg. Chem., 50 (2011) 836-846.

[10] (a) J.Y. Guo, T.L. Zhang, Y.H. Liu, K.B. Yu, Chinese J. Inorg. Chem., 22 (2006) 995-999;
(b) M.L. Guo, C.H. Guo, Acta Cryst. , 64 (2008) m342-344;
(c) H.M. Li, H.B. Yuan, S.Y. Yang, R.B. Huang, Acta Cryst. , 66 (2010) m983-984;
(d) Y.T. Li, C.W. Yan, Pol. J. Chem., 76 (2002) 765-771.

[11] (a) T. Fukushima, S. Horike, H. Kobayashi, M. Tsujimoto, S. Isoda, M.L. Foo, Y. Kubota, M. Takata, S. Kitagawa, J. Am. Chem. Soc., 134 (2012) 13341-13347;
(b) J.P. Mowat, S.R. Miller, J.M. Griffin, V.R. Seymour, S.E. Ashbrook, S.P. Thompson, D. Fairen-Jimenez, A.M. Banu, T. Duren, P.A. Wright, Inorg. Chem., 50 (2011) 10844-10858.

[12] K. Uemura, Y. Yamasaki, F. Onishi, H. Kita, M. Ebihara, Inorg. Chem., 49 (2010) 10133-10143.

[13] H.-P. Xiao, X.-H. Li, Q. Shi, W.-B. Zhang, J.-G. Wang, A. Morsali, J. Coord. Chem., 61 (2008) 2905-2915.

[14] (a) S.P. Chen, Y.X. Ren, W.T. Wang, S.L. Gao, Dalton Trans., 39 (2010) 1552-1557;
(b) J. Ye, J. Zhang, G. Ning, G. Tian, Y. Chen, Y. Wang, Cryst. Growth Des., 8 (2008) 3098-3106; (c)
X. Zhang, Q. Fang, G. Zhu, J. Molec. Struct., 969 (2010) 208-215.

[15] Y.T. Li, J. Zhang, C.W. Yan, Pol. J. Chem., 77 (2003) 797-804.

[16] R.C. Severance, M.D. Smith, H.C. zur Loye, Inorg. Chem., 50 (2011) 7931-7933.

[17] R.C. Severance, M.D. Smith, H.-C. zur Loye, Solid State Sci., 14 (2012) 725-729.

[18] Bruker, Bruker AXS Inc, Madison (WI), USA (2009).

[19] Z. Otwinowski, W. Minor, *Methods Enzymol.*, in: Macromolecular Crystallography, part A, Academic Press, New York, 1997, pp. 307-327.

[20] A. Altomare, M.C. Burla, M. Camalli, G.L. Cascarano, C. Giacovazzo, A. Guagliardi, A.G.G. Moliterni, G. Polidori, R. Spagna, J. Appl. Cryst., 32 (1999) 115 - 119.

[21] (a) C.B. Hübschle, G.M. Sheldrick, B. Dittrich, J. Appl. Cryst., 44 (2011) 1281-1284; (b) G.M. Sheldrick, Acta Cryst. , C71 (2015) 3-8.

[22] J.A. Smith, M.J. Singh-Wilmot, K.P. Carter, C.L. Cahill, A.J. Lough, C.S. Knee, New J. Chem., 40 (2016) 7338-7349.

[23] D.A. Brown, J. Edwards, J. Chem. Soc., Dalton: Inorg. Chem., 16 (1972-1999) 1757-1762.

[24] R.D. Shannon, Acta Cryst., A32 (1976) 751-768.

[25] G.B. Deacon, R.J. Phillips, Coord. Chem. Rev., 33 (1980) 227–250.

[26] E.G. Bakalbassis, C.A. Tsipis, Inorg . Chem., 24 (1985) 4233-4234.